SEE CORRECTION FOR THIS ARTICLE

Wettability effect on nanoconfined water flow

Keliu Wu[a,1], Zhangxin Chen[a,1], Jing Li[b], Xiangfang Li[b], Jinze Xu[a], and Xiaohu Dong[a,b]

[a]Department of Chemical and Petroleum Engineering, University of Calgary, Calgary, AB T2N 1N4, Canada; and [b]Key Laboratory for Petroleum Engineering of the Ministry of Education, China University of Petroleum, Beijing 102249, China

Edited by David A. Weitz, Harvard University, Cambridge, MA, and approved February 15, 2017 (received for review July 30, 2016)

Understanding and controlling the flow of water confined in nanopores has tremendous implications in theoretical studies and industrial applications. Here, we propose a simple model for the confined water flow based on the concept of effective slip, which is a linear sum of true slip, depending on a contact angle, and apparent slip, caused by a spatial variation of the confined water viscosity as a function of wettability as well as the nanopore dimension. Results from this model show that the flow capacity of confined water is 10^{-1}~10^{7} times that calculated by the no-slip Hagen–Poiseuille equation for nanopores with various contact angles and dimensions, in agreement with the majority of 53 different study cases from the literature. This work further sheds light on a controversy over an increase or decrease in flow capacity from molecular dynamics simulations and experiments.

nanoconfined water flow | nanopores | wettability | slip | viscosity

The flow behavior of water confined in nanopores is crucial for understanding and resolving many common challenging problems in science and engineering, such as nanomedicine (1), water purification (2), and energy storage and conversion (3–5), as well as geophysical processes (6, 7). A practical investigation of the confined water flow has been facilitated due to the availability of new tools (8–13) and recent advances in nanofabrication (14–16), which can be used to validate a novel theory of fluid flow at the nanoscale.

Many investigations have shown that properties of confined water differ drastically from those of bulk water (17–22), as a result of the varying structure and dynamics of the confined water induced by an interaction from nanopore walls (23–26). Moreover, these physical phenomena are further augmented by a high ratio of nanopore walls to a confined water volume (4). Some novel and different flow phenomena have been discovered, helping in theoretical investigations of the dynamics of the confined water. The flow rates, measured by Majumder et al. (27) and Holt et al. (14) for water flow through membranes of carbon nanotubes (CNTs) with diameters of 1.3–7.0 nm, are two to five orders of magnitude greater than those calculated by the no-slip Hagen–Poiseuille equation. However, the flow rate of water through 44-nm carbon nanopipes, measured by Whitby et al. (28), is only an order of magnitude greater. Furthermore, a decrease in the flow rate can occur for water confined in some nanopores, which has been discovered by many investigators (29–32). These huge differences may arise from the significantly different strength of an interaction between water and nanopore walls, which strongly depends on the contact angle of water on these walls (2, 33).

Although the flow behavior of confined water is mainly dominated by an interaction between water and nanopore walls (24, 34) and is substantially different from that occurring in microscale pores (35–37), a continuum (i.e., macroscopic) description combined with a molecular dynamics (MD) (microscopic) description may be valid for modeling flow of water confined in nanopores with a diameter of larger than 1.6 nm (4) because the microscale and nanoscale pores possess similar primary flow mechanisms (38, 39). However, important emerging new physical phenomena must be taken into account in the latter (40, 41), including different boundary conditions (slip, no-slip, and multilayer sticking) (30) and apparent viscosity caused by an interaction between water and nanopore walls (42, 43). Here we propose a simple model for confined water flow based on the concept of effective slip, which is a linear sum of true slip, as a function of a contact angle, and apparent slip, arising from the varying viscosity of the confined water. We establish a relationship between a true slip length and wettability as well as the links between an apparent slip length, wettability, and a nanopore dimension. The flow rates calculated by this model are in accord with the majority of those from the literature for water confined in nanopores, with a total of 53 cases. This model can be used to quantitatively explain a controversy in MD simulations and experiments over an increase or decrease in the flow capacity of confined water. This study provides a simple and effective tool for modeling flow of water confined in nanopores with a diameter of larger than 1.6 nm.

Results

Mechanisms of Water Flow Through Nanopores. Many issues related to mechanisms of water flow in nanopores are still unresolved, even including the most basic one: How does the water slip actually happen? (43). Unfortunately, to the best of our knowledge, no satisfactory answer can be given at present. We summarize the basic physics underlying these issues and make full use of all experimental evidence collected in the literature to reveal the most accredited mechanisms of water flow through nanopores.

The confined water possesses unique structural and dynamical properties, significantly different from those of bulk water (23, 24). It is now clear that water confined in nanopores can exhibit a dramatic change in viscosity (44–46), and the no-slip boundary condition is not always universal (14, 27, 43, 47). This is because the viscosity and slip of the confined water strongly depend on a relative strength of two interactions, namely, a ratio of the water–wall interaction to the water intermolecular interaction (25, 48). Generally, for the water confined in hydrophilic nanopores with a ratio higher than unity, a substantial epitaxial ordering of water is induced and some fluid layers, whose thickness increases with an increasing strength in the water–wall interaction, become locked to the walls (49); hence, the viscosity of water in the vicinity of a wall is higher than that of bulk water (50, 51), and a no-slip boundary condition, which is also named multilayer sticking (30), is valid (Fig. 1 *A* and *B*). For the

Significance

The flow of water confined in nanopores is significantly different from that of bulk water. Moreover, understanding and controlling the flow of the confined water remains an open question, especially concerning whether the flow capacity of the confined water increases or not compared with that of bulk water. Here, combining a theoretical analysis and data from molecular dynamics simulations and experiments in the literature we develop a simple model for the flow of water confined in nanopores. We find that a contact angle and a nanopore dimension may substantially affect the confined water flow. We also quantitatively explain a controversy over an increase or decrease in flow capacity.

Author contributions: K.W. and Z.C. designed research; K.W. and Z.C. performed research; J.L., X.L., J.X., and X.D. analyzed data; and K.W. and Z.C. wrote the paper.

The authors declare no conflict of interest.

This article is a PNAS Direct Submission.

[1]To whom correspondence may be addressed. Email: wukeliu19850109@163.com or zhachen@ucalgary.ca.

This article contains supporting information online at www.pnas.org/lookup/suppl/doi:10.1073/pnas.1612608114/-/DCSupplemental.

Downloaded from https://www.pnas.org by 147.161.165.28 on March 4, 2025 from IP address 147.161.165.28.

water confined in midwetting nanopores the ratio likely equals unity, and the no-slip boundary condition still holds, whereas the viscosity of water near walls decreases due to an existing depletion region near the walls (52) (Fig. 1*C*). However, for the water confined in hydrophobic nanopores with a ratio smaller than unity, the assumption of the no-slip boundary condition breaks down (53); in other words, water molecules can move directly along walls (54, 55), which can be described by a true slip length, and, furthermore, the viscosity of water near the walls significantly decreases (56) (Fig. 1 *D* and *E*).

The viscosity of the confined water, which is a function not only of wall properties but also a nanopore dimension (57), and the true slip length play a crucial role in the flow behavior of water confined in nanopores. Here, the true slip length $l_{s,t}$, defined in the standard partial slip boundary condition, is a ratio of the slip velocity to the shear rate at the effective hydrodynamic boundary position, and thus it cannot be negative; additionally, the effect of a varying viscosity on the confined water flow can be treated by an apparent slip length modeled by a continuum theory, as shown in $l_{s,a}$ in Fig. 1.

True Slip Versus Wettability. The flow of confined water depends strongly on the slip length, and an accurate modeling of the water flow at the nanoscale depends on reliable calculations and/or measurements of this quantity. Whether the true slip of water near nanopore walls occurs is a result of the water–wall interaction. The strength of this interaction can be characterized by wettability (47). Hence, there exists a relationship between true slip and wettability for the majority of water–wall systems. By this physically motivated argument, the true slip length of water as a scaling function of a contact angle can be described as (58)

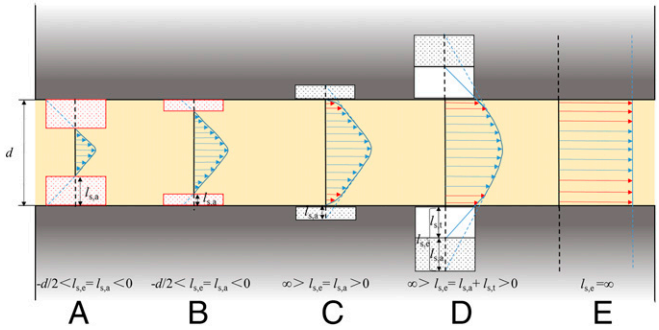

Fig. 1. Schematic representation of water flow in nanopores. From *A* to *E*, the strength of a water–wall interaction decreases and the contact angle increases. True slip occurs at a molecular level, where water molecules are effectively sliding on walls, and its value $l_{s,t}$ cannot be negative. Apparent slip does not occur on walls but at water/water interfaces due to the varying viscosity of water near the walls, and its value $l_{s,a}$ can be negative or positive depending on the wall wettability. Effective slip, a linear sum of true slip and apparent slip, refers to the case where true and/or apparent slip is estimated by an appropriate method (averaging) without tedious calculations for modeling the confined water flow, and its value $l_{s,e}$ can be negative, zero, or positive. (*A* and *B*) Apparent slip with a negative slip length, where the water–wall interaction is larger than the water intermolecular interaction, and red squares are the regions with high viscosity at which the water molecules keep static relative to the walls. (*C*) Apparent slip with a positive slip length, where the water–wall interaction equals the water intermolecular interaction, and red arrows are the regions with low viscosity due to the existing depletion regions. (*D* and *E*) Apparent and true slip with both positive slip lengths, where the water–wall interaction is smaller than the water intermolecular interaction, and red arrows are the regions with low viscosity. Note that effective slip equals apparent slip due to the true slip of zero in *A*, *B* and *C*, whereas its value is a linear sum of apparent and true slip lengths with a finite and infinite slip length in *D* and *E*, respectively.

$$l_{s,t} = C/(\cos\theta + 1)^2, \quad [1]$$

where $l_{s,t}$ is the true slip length of water at walls, θ is the contact angle (a calculation method is provided in *SI Appendix*, *SI Text*, section A), and C is a constant for a liquid, fitted with experimental or MD simulation data. Note that C as a constant is only valid for a liquid with a constant viscosity, and we assume that it is also a constant in this work.

To calculate accurately the true slip length, a curve with $C = 0.41$ fitted by the MD simulation data should be adopted rather than that by the experimental data, as shown in *SI Appendix*, *SI Text*, section B, because a measured value from experimental data is an effective slip length as a function of many factors, such as wall wettability (59), wall roughness (48), nanobubbles (60), operation conditions (32), and fluid viscosity (61). One should pay much attention to the accurate determination of a contact angle higher than 145° because its small error can contribute a huge variation in the true slip length (*SI Appendix*, Fig. S1). It is noted that the true slip length is not exclusively controlled by the wall wettability, which has been confirmed by many scholars (49, 62–67), as shown in *SI Appendix*, *SI Text*, section B. Thus, one uses Eq. **1** with the utmost caution. In addition, the true slip length, determined by Eq. **1**, is on the basis of MD simulation data for an unconfined liquid with a constant viscosity.

Viscosity Versus Wettability and Confinement. The true slip length is small, 0–25 nm for contact angles of 0–150° (*SI Appendix*, Fig. S1). However, Majumder et al. (27) published a paper that indicated that an effective slip length ranging from 39 to 68 μm would be required to reproduce the measured water flow rates in 7-nm aligned, multiwalled carbon nanotubes (MWCNTs). In the following year, Holt et al. (14) measured water flow rates through 1.3- to 2.0-nm double-walled carbon nanotubes (DWNTs), and the required effective slip lengths were found to be up to 1.4 μm. Moreover, an effective slip length can even be a negative value, which is also named multilayer sticking, indicating that several adsorbed layers are immobilized at walls. The experiments by Chan and Horn (29) provided strong evidence in this case. Hence, in addition to true slip, other unique physics need to be responsible for the existing wide range of effective slip lengths. The apparent slip, caused by a varying viscosity of confined water, may be the most accredited one of them. Many experiments (11, 50) and MD simulations (57, 68, 69) have demonstrated that the viscosity of the confined water is spatially varying, which stems from the variations of structural and dynamical properties of the confined water as a result of the interaction force exerted by nanopore walls (70).

To obtain an effective viscosity of the confined water a weighted average of the viscosities in the interface and bulk-like regions in nanopores is adopted (68):

$$\mu(d) = \mu_i \frac{A_i(d)}{A_t(d)} + \mu_\infty \left[1 - \frac{A_i(d)}{A_t(d)}\right], \quad [2]$$

where μ_i and A_i are the water viscosity and area of the interface region, respectively, μ_∞ is the viscosity of bulk water, A_t is the total cross-sectional area, and d is the nanopore diameter.

The effective viscosity strongly depends on the water viscosity and area of an interface region. The area of the interface region can be calculated by a critical thickness, which is defined as one above which water is expected to behave like bulk water without being affected by an interaction from walls. The critical thickness can be determined as 0.7 nm on the basis of spatially varying structure and dynamics of the confined water by experiments and/or MD simulations, as shown in *SI Appendix*, *SI Text*, section C and Table S1. The water viscosity in the interface region, also strongly affected by the interaction from walls, is a function of a contact angle. Based on the results from experiments and MD

Downloaded from https://www.pnas.org by 147.161.165.28 on March 4, 2025 from IP address 147.161.165.28.

simulations (50, 68, 71–80) (Fig. 2), a linear relationship between the ratio μ_i/μ_∞ and the contact angle can be correlated as

$$\frac{\mu_i}{\mu_\infty} = -0.018\theta + 3.25. \quad [3]$$

The viscosity in the interface region increases as the contact angle decreases, because the stronger the interaction from walls the denser a hydrogen bonding network and the more ordered and stable structure that yields stronger hydrogen bonds in the interface region (72). Also, compared with bulk water, the water viscosity in the interface region is smaller or larger for the water confined in hydrophobic (78) or hydrophilic (71, 73, 74) nanopores, respectively, as shown in Fig. 2.

Several points are noteworthy. First, in fact, the viscosity in the interfacial region is not constant but is a function of confinement (78); as the nanopore diameter decreases, it increases for nanopores with hydrophilic walls (44), whereas it decreases for nanopores with hydrophobic walls (79). Second, the viscosity in the interfacial region can be three to six orders of magnitude higher than the bulk water viscosity for a nanopore with a diameter smaller than 1 nm and hydrophilic walls (11, 44), whereas it decreases very quickly but is still larger than bulk water viscosity when the nanopore diameter is larger than 1 nm (71). Third, we assume that the viscosity in the interfacial region in Eq. **3** is a constant for a nanopore with fixed wettability and a diameter of larger than 1.4 nm, as shown in Fig. 2. Thus, Eq. **3** is only applicable in water confined in a nanopore with a diameter of larger than 1.4 nm. Fourth, the behavior of water flow through a nanopore with a diameter of smaller than 1.4 nm changes very quickly with the diameter due to a dramatically varying viscosity in the interfacial region (71), and thus determining the water viscosity in the interfacial region becomes key to model flow behavior at this small nanoscale. Finally, classical MD simulations may be unable to represent the interfacial dynamics well at a quantitative level due to their limitations, although they can do so at a qualitative level. Therefore, we should exercise exceptional care in adopting the water viscosity in the interfacial region obtained by MD simulations for nanopores with a diameter of smaller than 1 nm, although MD simulations are able to reproduce the viscosity for nanopores with a diameter of larger than 1 nm (81), and thus MD simulations are relatively reliable in modeling the water flow using the viscosity obtained by them. A further literature review on the water viscosity in the interfacial region is included in *SI Appendix*, *SI Text*, section D.

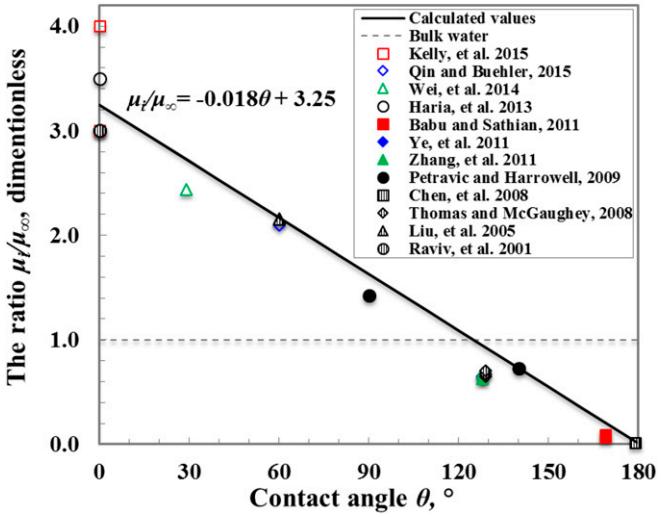

Fig. 2. The dependence of the water viscosity in the interface region on wettability.

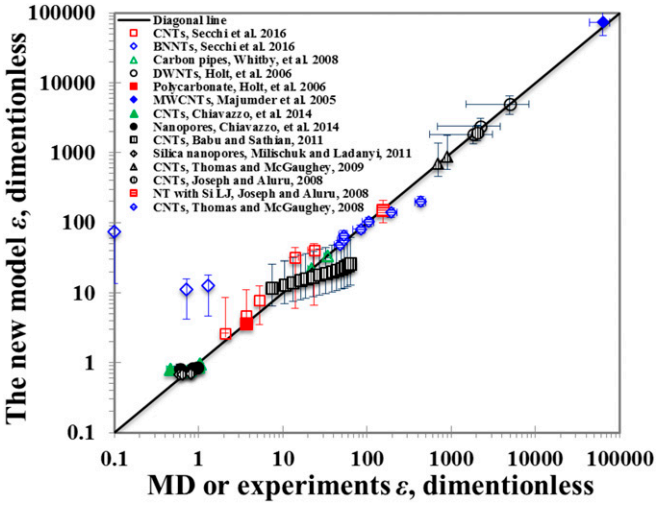

Fig. 3. Comparison of the enhancement factors calculated by our model with data from experiments and MD simulations in the literature. Fifty-three cases, composed of 15 cases from experiments and 38 cases from MD simulations, are included for the model validation. Nanopores from the experiments are five different CNTs with dimensions (nanometers) of (R_t, L_t) = (15, 700), (17, 450), (33, 900), (38, 800) and (50, 1,000) and three different boron nitride nanotubes (BNNTs) with dimensions (nanometers) of (R_t, L_t) = (23, 600), (26, 700) and (7, 1,300), where R_t and L_t are the radius and length of nanotubes, respectively (67); 44-nm-diameter carbon pipes (28); three DWNTs membranes with pore diameters ranging from 1.3 to 2.0 nm and a polycarbonate membrane with a pore diameter of 15 nm (14); and an aligned MWCNT membrane with a pore diameter of about 7 nm (27). Nanopores from the MD simulations are single-walled CNTs and nanopores (13), single-walled CNTs with diameters ranging from 1.62 to 3.06 nm (75), cylindrical pores in amorphous silica with diameters ranging from 2 to 4 nm (82), 75- and 150-nm-long CNTs (39), 2.17-nm-diameter CNTs and a nanotube with the same smooth structure as CNTs but with much more attractive Lennard-Jones (LJ) parameters of silicon (nanotubes with Si LJ) (52), and CNTs with diameters ranging from 1.66 to 4.99 nm (68). A diagonal line is a guided eye line for convenient comparison. Our model is able to recover the majority of cases from the literature. It is unable to predict the enhancement factors for the 3 BNNTs from ref. 67, because the true slip length is not controlled by the wetting properties for BNNTs, as discussed above. In addition, for the five CNTs from Secchi et al. (67) the enhancement factors predicted by our model are slightly greater than the experimental results, and this may be caused by the fact that our present model neglects end effects, which may play a role in the nanoconfined water flow due to a relatively small ratio of a tube length to its radius with a relatively large slip length. The error bars of ε by our model are determined from the errors of determining the contact angles for nanopore walls.

The effective viscosity calculated by Eq. **2** matches very well with the results from MD simulations and experiments (*SI Appendix*, *SI Text*, section E). The effective viscosity is a function not only of a contact angle but also of confinement, because the interaction from walls becomes increasingly dominant as the pore dimension shrinks to a nanoscale region, which causes the portion of water molecules in the interface region to increase relative to the total water molecules present in nanopores (28).

Water Flow Through Nanopores. It may be feasible that the water flow through nanopores is modeled by the continuum fluid mechanics when the characteristic flow dimension is larger than 1.6 nm (38, 39). However, the extent of departure from what is predicted by the no-slip Hagen–Poiseuille equation is huge (14, 27) due to a velocity "jump" at walls and the varying water molecule orientations and hydrogen bonds in an interface region. Based on the no-slip Hagen–Poiseuille equation, Holt et al.

Downloaded from https://www.pnas.org by 147.161.165.28 on March 4, 2025 from IP address 147.161.165.28.

Table 1. Data from experimental results reproduced by the model in Fig. 3

Ref.	Pore material	Pore geometry	Pore diameter, nm	Pore length, nm
Secchi et al. (67)	CNTs	Cylindrical geometry	30–100	450–1,000
Secchi et al. (67)*	BNNTs	Cylindrical geometry	14–52	600–1,300
Whitby et al. (28)	Carbon pipes	Cylindrical geometry	44 ± 3	78,000 ± 2,000
Holt et al. (14)	DWNTs	Cylindrical geometry	1.3–2.0	2,000–3,000
Holt et al. (14)	Polycarbonate	Cylindrical geometry	15	6,000
Majumder et al. (27)	MWCNTs	Cylindrical geometry	~7	34,000

*Our model is unable to reproduce the experimental enhancement factors for the BNNTs because their true slip lengths are not controlled by their wetting properties.

(14) considered the water slip at walls and modeled the water flow with a pressure gradient $\partial p/\partial z$ through nanopores as

$$Q_s = \frac{\pi}{8\mu_\infty}\left[(d/2)^4 + 4(d/2)^3 l_{s,t}\right]\frac{\partial p}{\partial z}. \quad [4]$$

It is noted that Eq. **4** adopts the viscosity of bulk water and is unable to consider the effect of the varying effective viscosity for different nanopores on the confined water flow. Here, we simultaneously take the slip and effective viscosity into account, and the confined water flux becomes

$$Q_s = \frac{\pi}{8\mu(d)}\left[(d/2)^4 + 4(d/2)^3 l_{s,t}\right]\frac{\partial p}{\partial z}. \quad [5]$$

For Eq. **5** it is worthy to note that (i) the effective viscosity $\mu(d)$ is a constant in a water–nanopore system with a specific dimension and wettability and (ii) the true slip length $l_{s,t}$, considering the effect of wettability, approximately represents the effect of slip depending on the local velocity profile at the wall of a nanopore.

If we keep the viscosity of bulk water with the same form of Eq. **4**, the slip length $l_{s,t}$ in Eq. **4** should be replaced by the effective slip length $l_{s,e}$. Comparing Eq. **5** with Eq. **4**, the effective slip length is expressed as

$$l_{s,e} = l_{s,a} + l_{s,t} = \left[\frac{\mu_\infty}{\mu(d)} - 1\right]\left(\frac{d}{8} + l_{s,t}\right) + l_{s,t}. \quad [6]$$

Eq. **6** shows that the effective slip length can be expressed by a linear sum of the apparent and true slip lengths.

The enhancement factor, indicated by Majumder et al. (27) and Holt et al. (14), is defined as the ratio of the measured flow flux to Q_n, predicted by the Hagen–Poiseuille equation using a bulk viscosity and the no-slip boundary condition. If the measured flow flux is modeled by Eq. **5**, the enhancement factor is

$$\varepsilon = \frac{Q_s}{Q_n} = \left[1 + 8\frac{l_{s,t}}{d}\right]\frac{\mu_\infty}{\mu(d)}. \quad [7]$$

Fig. 3 shows the comparison of the results by our model and those from 53 different cases, composed of 15 cases from experiments (14, 27, 28, 67) and 38 cases from MD simulations (13, 39, 52, 68, 75, 82) in the literature, and a summary of experimental data are listed in Table 1 (various parameters used to reproduce Fig. 3 are shown in *SI Appendix*, Table S2). Here, for the water confined in nanopores with diverse types and dimensions, although a wide range of enhancement factors span over six orders of magnitude, this model is still able to simulate accurately the majority of these confined water flows, which suggests that it successfully captures or reflects the underlying physics behind these different flow behaviors, including the water structure and dynamics and the three boundary conditions of multilayer sticking, no-slip, and slip at walls.

Discussion

Fig. 4 shows the main conclusive results in this study, namely the dependence of the confined water flow on wettability and confinement.

In particular, our results demonstrate that the flow capacity of confined water can decrease one order of magnitude because of multilayer sticking, whereas it can increase up to seven orders

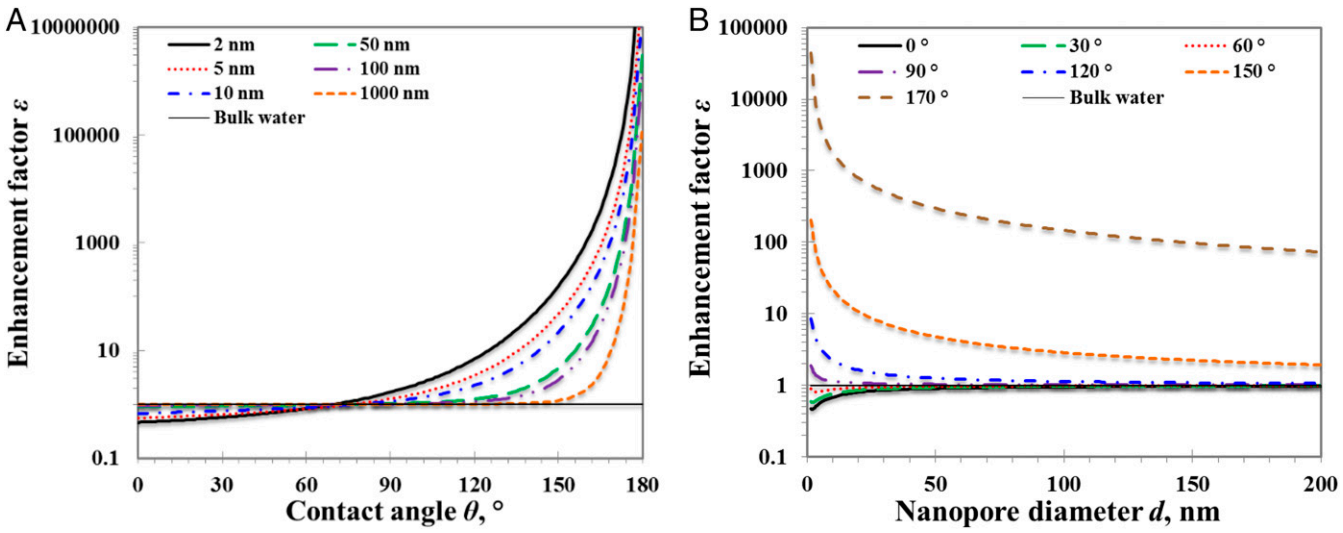

Fig. 4. The dependence of an enhancement factor on nanopore properties. (*A*) Enhancement factor versus contact angle. (*B*) Enhancement factor versus nanopore diameter.

Downloaded from https://www.pnas.org by 147.161.165.28 on March 4, 2025 from IP address 147.161.165.28.

of magnitude due to the effective slip compared with that of bulk water for nanopores with a wide range of wettability here investigated, as shown in Fig. 4*A*. The huge difference in the enhancement factor is caused by the significantly different strength of the interaction from nanopore walls. The stronger the interaction the larger the activated energy needed for the molecular motion of the confined water (24, 83). These results reconcile the two contradictory trends of a flow capacity variation of the water confined in various nanopores, namely, a debatable issue that the flow capacity of the confined water decreases or increases compared with that of bulk water. Furthermore, they show that not only nearly frictionless walls (34, 84) and nanobubbles (48, 85, 86) but also strong hydrophobic walls are able to enhance enormously the flux of the confined water.

In addition, a small difference in the nanopore dimension has a big effect on the confined water flow due to the strong dependence of the structure and dynamics of the confined water on the dimension (87), especially for nanopores with a diameter smaller than 10 nm, as shown in Fig. 4*B*. Similar results have been observed in many experiments. The enhancement factor for the confined water through 44-nm carbon pipes measured by Whitby et al. (28) is much smaller than those observed through the smaller CNTs with diameters of 7 nm and smaller than 2 nm by Majumder et al. (27) and Holt et al. (14), respectively, although it is nevertheless substantial over an order of magnitude (18–35), implying that the unique phenomena of the confined water flow occur to a significant extent even in relatively large nanopores. However, for the water confined in pores with a diameter of larger than 200 nm and a contact angle of smaller than 150°, the enhancement factor by our model is smaller than 2, which may provide a reason that Sinha et al. (88) did not detect enhancement of the water flow through nanopipes with diameters ranging from 200 to 300 nm.

Although the results by our model are possibly limited to a system of nanopores with ultrasmooth walls and the confined water without any dissolved gas or contaminant, the conclusions elucidate a general understanding of the flow behavior of water confined in nanopores with varying wettability and dimensions, which can have an important impact in some theoretical studies and industrial applications. Most importantly, the proposed model is simple and effective in modeling the confined water flow, which overcomes the main shortcomings of MD simulations with computational limitations (65, 75) and time-consuming experiments with high costs (35, 89). However, it is noted that our model does not consider end effects (90), which may cause an error in modeling the nanoconfined water flow for nanopores with a short geometric length of any friction or a low inner friction with any length (91). A further literature review on end effects is included in *SI Appendix, SI Text*, section F.

Conclusions

In summary, we have investigated the flow of water confined in nanopores with different wettability and dimensions by the combination of a theoretical analysis and data from MD simulations and experiments in the literature. Our results have demonstrated that the effective slip length is a crucial parameter controlling the flow of the confined water, which is a linear sum of the true and apparent slip lengths. Here, the true slip length depends on a contact angle, whereas the apparent slip length, caused by a spatial variation of the confined water viscosity, is a function of wettability as well as the dimension. A model is proposed from the modified Hagen–Poiseuille equation, taking the wettability and dimension into account, and is successfully applied to model the confined water flow with a wide range of enhancement factors of 10^{-1} to 10^{7}. The results by this model are in agreement with the majority of 53 different cases from the literature. This model is also able to quantitatively explain a controversy in MD simulations and experiments over an increase or decrease in flow capacity. This work further demonstrates the effectiveness of the continuum fluid mechanics and provides a simple and valuable tool in modeling the flow of water confined in nanopores with a diameter larger than 1.6 nm.

Methods

Idea of the Model. We model the confined water flow by considering viscous flow resistance and water–wall interface resistance. The viscous flow resistance is described by apparent slip stemming from a spatial variation of the confined water viscosity, and the water–wall interface resistance is characterized by true slip.

Calculation of a True Slip Length. We assume that the true slip length is a function of a contact angle and calculate it by using Eq. **1** with $C = 0.41$ fitted by the MD simulation data rather than that by the experimental data. More details are included in *SI Appendix, SI Text*, section B.

Calculation of an Apparent Slip Length. We can obtain the apparent slip length by Eq. **6** with a known effective viscosity. We calculate an effective viscosity of the confined water by a weighted average of the viscosities in the interface and bulk-like regions in nanopores. The effective viscosity strongly depends on the water viscosity and area of an interface region. The water viscosity in the interface region is obtained by Eq. **3**, and the area of the interface region is calculated by a critical thickness of 0.7 nm, as shown in *SI Appendix, SI Text*, section C and Table S1.

ACKNOWLEDGMENTS. We thank the two anonymous reviewers for helpful reviews. This work was supported by the Natural Sciences and Engineering Research Council of Canada, Alberta Innovates – Energy and Environment Solutions, Foundation CMG, Alberta Innovates – Technology Futures Chairs, iCore, and the Frank and Sarah Meyer Foundation CMG Collaboration Centre (K.W., Z.C., J.X., and X.D.) and by National Natural Science Foundation of China Grants 51490654 and 51374222 (to J.L. and X.L.).

1. Sanhai WR, Sakamoto JH, Canady R, Ferrari M (2008) Seven challenges for nanomedicine. *Nat Nanotechnol* 3(5):242–244.
2. Shannon MA, et al. (2008) Science and technology for water purification in the coming decades. *Nature* 452(7185):301–310.
3. Aricò AS, Bruce P, Scrosati B, Tarascon JM, van Schalkwijk W (2005) Nanostructured materials for advanced energy conversion and storage devices. *Nat Mater* 4(5): 366–377.
4. Sparreboom W, van den Berg A, Eijkel JCT (2009) Principles and applications of nanofluidic transport. *Nat Nanotechnol* 4(11):713–720.
5. Siria A, et al. (2013) Giant osmotic energy conversion measured in a single transmembrane boron nitride nanotube. *Nature* 494(7438):455–458.
6. Warner NR, et al. (2012) Geochemical evidence for possible natural migration of Marcellus Formation brine to shallow aquifers in Pennsylvania. *Proc Natl Acad Sci USA* 109(30):11961–11966.
7. Keranen KM, Weingarten M, Abers GA, Bekins BA, Ge S (2014) Induced earthquakes. Sharp increase in central Oklahoma seismicity since 2008 induced by massive wastewater injection. *Science* 345(6195):448–451.
8. Naguib N, et al. (2004) Observation of water confined in nanometer channels of closed carbon nanotubes. *Nano Lett* 4(11):2237–2243.
9. Lasne D, et al. (2008) Velocity profiles of water flowing past solid glass surfaces using fluorescent nanoparticles and molecules as velocity probes. *Phys Rev Lett* 100(21): 214502.
10. Mirsaidov UM, Zheng H, Bhattacharya D, Casana Y, Matsudaira P (2012) Direct observation of stick-slip movements of water nanodroplets induced by an electron beam. *Proc Natl Acad Sci USA* 109(19):7187–7190.
11. Ortiz-Young D, Chiu HC, Kim S, Voïtchovsky K, Riedo E (2013) The interplay between apparent viscosity and wettability in nanoconfined water. *Nat Commun* 4: 2482.
12. Huang JY, et al. (2013) Nanowire liquid pumps. *Nat Nanotechnol* 8(4):277–281.
13. Chiavazzo E, Fasano M, Asinari P, Decuzzi P (2014) Scaling behaviour for the water transport in nanoconfined geometries. *Nat Commun* 5:4565.
14. Holt JK, et al. (2006) Fast mass transport through sub-2-nanometer carbon nanotubes. *Science* 312(5776):1034–1037.
15. Karan S, Samitsu S, Peng X, Kurashima K, Ichinose I (2012) Ultrafast viscous permeation of organic solvents through diamond-like carbon nanosheets. *Science* 335(6067):444–447.
16. Surwade SP, et al. (2015) Water desalination using nanoporous single-layer graphene. *Nat Nanotechnol* 10(5):459–464.
17. Heuberger M, Zäch M, Spencer ND (2001) Density fluctuations under confinement: When is a fluid not a fluid? *Science* 292(5518):905–908.
18. Scatena LF, Brown MG, Richmond GL (2001) Water at hydrophobic surfaces: Weak hydrogen bonding and strong orientation effects. *Science* 292(5518):908–912.
19. Werder T, et al. (2001) Molecular dynamics simulation of contact angles of water droplets in carbon nanotubes. *Nano Lett* 1(12):697–702.

Downloaded from https://www.pnas.org by 147.161.165.28 on March 4, 2025 from IP address 147.161.165.28.

20. Levinger NE (2002) Chemistry. Water in confinement. *Science* 298(5599):1722–1723.
21. Rivera JL, McCabe C, Cummings PT (2002) Layering behavior and axial phase equilibria of pure water and water+ carbon dioxide inside single wall carbon nanotubes. *Nano Lett* 2(12):1427–1431.
22. Köfinger J, Hummer G, Dellago C (2008) Macroscopically ordered water in nanopores. *Proc Natl Acad Sci USA* 105(36):13218–13222.
23. Mashl RJ, Joseph S, Aluru NR, Jakobsson E (2003) Anomalously immobilized water: A new water phase induced by confinement in nanotubes. *Nano Lett* 3(5):589–592.
24. Liu Y, Wang Q, Zhang L, Wu T (2005) Dynamics and density profile of water in nanotubes as one-dimensional fluid. *Langmuir* 21(25):12025–12030.
25. Krott LB, Bordin JR, Barbosa MC (2015) New structural anomaly induced by nanoconfinement. *J Phys Chem B* 119(1):291–300.
26. Ma M, et al. (2015) Water transport inside carbon nanotubes mediated by phonon-induced oscillating friction. *Nat Nanotechnol* 10(8):692–695.
27. Majumder M, Chopra N, Andrews R, Hinds BJ (2005) Nanoscale hydrodynamics: enhanced flow in carbon nanotubes. *Nature* 438(7064):44 (abstr).
28. Whitby M, Cagnon L, Thanou M, Quirke N (2008) Enhanced fluid flow through nanoscale carbon pipes. *Nano Lett* 8(9):2632–2637.
29. Chan DY, Horn RG (1985) The drainage of thin liquid films between solid surfaces. *J Chem Phys* 83(10):5311–5324.
30. Heinbuch U, Fischer J (1989) Liquid flow in pores: Slip, no-slip, or multilayer sticking. *Phys Rev A Gen Phys* 40(2):1144–1146.
31. Granick S (1991) Motions and relaxations of confined liquids. *Science* 253(5026): 1374–1379.
32. Thompson PA, Troian SM (1997) A general boundary condition for liquid flow at solid surfaces. *Nature* 389(6649):360–362.
33. Voronov RS, Papavassiliou DV, Lee LL (2006) Boundary slip and wetting properties of interfaces: Correlation of the contact angle with the slip length. *J Chem Phys* 124(20): 204701.
34. Whitby M, Quirke N (2007) Fluid flow in carbon nanotubes and nanopipes. *Nat Nanotechnol* 2(2):87–94.
35. Lorenz UJ, Zewail AH (2014) Nanofluidics. Observing liquid flow in nanotubes by 4D electron microscopy. *Science* 344(6191):1496–1500.
36. Verweij H, Schillo MC, Li J (2007) Fast mass transport through carbon nanotube membranes. *Small* 3(12):1996–2004.
37. Nair RR, Wu HA, Jayaram PN, Grigorieva IV, Geim AK (2012) Unimpeded permeation of water through helium-leak-tight graphene-based membranes. *Science* 335(6067): 442–444.
38. Striolo A (2006) The mechanism of water diffusion in narrow carbon nanotubes. *Nano Lett* 6(4):633–639.
39. Thomas JA, McGaughey AJ (2009) Water flow in carbon nanotubes: Transition to subcontinuum transport. *Phys Rev Lett* 102(18):184502.
40. Monteiro PJ, Rycroft CH, Barenblatt GI (2012) A mathematical model of fluid and gas flow in nanoporous media. *Proc Natl Acad Sci USA* 109(50):20309–20313.
41. Falk K, Coasne B, Pellenq R, Ulm FJ, Bocquet L (2015) Subcontinuum mass transport of condensed hydrocarbons in nanoporous media. *Nat Commun* 6:6949.
42. Klein J, Kumacheva E (1995) Confinement-induced phase transitions in simple liquids. *Science* 269(5225):816–819.
43. Neto C, Evans DR, Bonaccurso E, Butt HJ, Craig VS (2005) Boundary slip in Newtonian liquids: A review of experimental studies. *Rep Prog Phys* 68(12):2859.
44. Goertz MP, Houston JE, Zhu XY (2007) Hydrophilicity and the viscosity of interfacial water. *Langmuir* 23(10):5491–5497.
45. Campbell SE, Luengo G, Srdanov VI, Wudl F, Israelachvili JN (1996) Very low viscosity at the solid–liquid interface induced by adsorbed C60 monolayers. *Nature* 382(6591): 520–522.
46. Li T, Gao J, Szoszkiewicz R, Landman U, Riedo E (2007) Structured and viscous water in subnanometer gaps. *Phys Rev B* 75(11):115415.
47. Cottin-Bizonne C, Barrat JL, Bocquet L, Charlaix E (2003) Low-friction flows of liquid at nanopatterned interfaces. *Nat Mater* 2(4):237–240.
48. Granick S, Zhu Y, Lee H (2003) Slippery questions about complex fluids flowing past solids. *Nat Mater* 2(4):221–227.
49. Thompson PA, Robbins MO (1990) Origin of stick-slip motion in boundary lubrication. *Science* 250(4982):792–794.
50. Raviv U, Laurat P, Klein J (2001) Fluidity of water confined to subnanometre films. *Nature* 413(6851):51–54.
51. Feibelman PJ (2013) Viscosity of ultrathin water films confined between aluminol surfaces of kaolinite: Ab initio simulations. *J Phys Chem C* 117(12):6088–6095.
52. Joseph S, Aluru NR (2008) Why are carbon nanotubes fast transporters of water? *Nano Lett* 8(2):452–458.
53. Barrat JL, Bocquet L (1999) Large slip effect at a nonwetting fluid-solid interface. *Phys Rev Lett* 82(23):4671.
54. Schoch RB, Han J, Renaud P (2008) Transport phenomena in nanofluidics. *Rev Mod Phys* 80(3):839–883.
55. Vinogradova OI, Koynov K, Best A, Feuillebois F (2009) Direct measurements of hydrophobic slippage using double-focus fluorescence cross-correlation. *Phys Rev Lett* 102(11):118302.
56. Vinogradova OI (1995) Drainage of a thin liquid film confined between hydrophobic surfaces. *Langmuir* 11(6):2213–2220.
57. Hoang H, Galliero G (2012) Local viscosity of a fluid confined in a narrow pore. *Phys Rev E Stat Nonlin Soft Matter Phys* 86(2 Pt 1):021202.
58. Huang DM, Sendner C, Horinek D, Netz RR, Bocquet L (2008) Water slippage versus contact angle: A quasiuniversal relationship. *Phys Rev Lett* 101(22):226101.
59. Schmatko T, Hervet H, Leger L (2005) Friction and slip at simple fluid-solid interfaces: The roles of the molecular shape and the solid-liquid interaction. *Phys Rev Lett* 94(24): 244501.
60. Steinberger A, Cottin-Bizonne C, Kleimann P, Charlaix E (2007) High friction on a bubble mattress. *Nat Mater* 6(9):665–668.
61. Doshi DA, Watkins EB, Israelachvili JN, Majewski J (2005) Reduced water density at hydrophobic surfaces: Effect of dissolved gases. *Proc Natl Acad Sci USA* 102(27): 9458–9462.
62. Joly L, Ybert C, Trizac E, Bocquet L (2006) Liquid friction on charged surfaces: From hydrodynamic slippage to electrokinetics. *J Chem Phys* 125(20):204716.
63. Suk ME, Raghunathan AV, Aluru NR (2008) Fast reverse osmosis using boron nitride and carbon nanotubes. *Appl Phys Lett* 92(13):133120.
64. Hilder TA, Gordon D, Chung SH (2009) Salt rejection and water transport through boron nitride nanotubes. *Small* 5(19):2183–2190.
65. Ho TA, Papavassiliou DV, Lee LL, Striolo A (2011) Liquid water can slip on a hydrophilic surface. *Proc Natl Acad Sci USA* 108(39):16170–16175.
66. Tocci G, Joly L, Michaelides A (2014) Friction of water on graphene and hexagonal boron nitride from ab initio methods: Very different slippage despite very similar interface structures. *Nano Lett* 14(12):6872–6877.
67. Secchi E, et al. (2016) Massive radius-dependent flow slippage in carbon nanotubes. *Nature* 537(7619):210–213.
68. Thomas JA, McGaughey AJ (2008) Reassessing fast water transport through carbon nanotubes. *Nano Lett* 8(9):2788–2793.
69. Neek-Amal M, Peeters FM, Grigorieva IV, Geim AK (2016) Commensurability effects in viscosity of nanoconfined water. *ACS Nano* 10(3):3685–3692.
70. Thomas JA, McGaughey AJH (2007) Effect of surface wettability on liquid density, structure, and diffusion near a solid surface. *J Chem Phys* 126(3):034707.
71. Kelly S, Balhoff MT, Torres-Verdín C (2015) Quantification of bulk solution limits for liquid and interfacial transport in nanoconfinements. *Langmuir* 31(7):2167–2179.
72. Qin Z, Buehler MJ (2015) Nonlinear viscous water at nanoporous two-dimensional interfaces resists high-speed flow through cooperativity. *Nano Lett* 15(6):3939–3944.
73. Wei N, Peng X, Xu Z (2014) Breakdown of fast water transport in graphene oxides. *Phys Rev E Stat Nonlin Soft Matter Phys* 89(1):012113.
74. Haria NR, Grest GS, Lorenz CD (2013) Viscosity of nanoconfined water between hydroxyl basal surfaces of kaolinite: Classical simulation results. *J Phys Chem C* 117(12): 6096–6104.
75. Babu JS, Sathian SP (2011) The role of activation energy and reduced viscosity on the enhancement of water flow through carbon nanotubes. *J Chem Phys* 134(19):194509.
76. Ye H, Zhang H, Zhang Z, Zheng Y (2011) Size and temperature effects on the viscosity of water inside carbon nanotubes. *Nanoscale Res Lett* 6(1):87.
77. Zhang H, Ye H, Zheng Y, Zhang Z (2011) Prediction of the viscosity of water confined in carbon nanotubes. *Microfluid Nanofluidics* 10(2):403–414.
78. Petravic J, Harrowell P (2009) Spatial dependence of viscosity and thermal conductivity through a planar interface. *J Phys Chem B* 113(7):2059–2065.
79. Chen X, et al. (2008) Nanoscale fluid transport: Size and rate effects. *Nano Lett* 8(9): 2988–2992.
80. Liu Y, Wang Q, Wu T, Zhang L (2005) Fluid structure and transport properties of water inside carbon nanotubes. *J Chem Phys* 123(23):234701.
81. Bocquet L, Charlaix E (2010) Nanofluidics, from bulk to interfaces. *Chem Soc Rev* 39(3): 1073–1095.
82. Milischuk AA, Ladanyi BM (2011) Structure and dynamics of water confined in silica nanopores. *J Chem Phys* 135(17):174709.
83. Carrasco J, Hodgson A, Michaelides A (2012) A molecular perspective of water at metal interfaces. *Nat Mater* 11(8):667–674.
84. Skoulidas AI, Ackerman DM, Johnson JK, Sholl DS (2002) Rapid transport of gases in carbon nanotubes. *Phys Rev Lett* 89(18):185901.
85. Choi CH, Kim CJ (2006) Large slip of aqueous liquid flow over a nanoengineered superhydrophobic surface. *Phys Rev Lett* 96(6):066001.
86. Feuillebois F, Bazant MZ, Vinogradova OI (2009) Effective slip over superhydrophobic surfaces in thin channels. *Phys Rev Lett* 102(2):026001.
87. Koga K, Gao GT, Tanaka H, Zeng XC (2001) Formation of ordered ice nanotubes inside carbon nanotubes. *Nature* 412(6849):802–805.
88. Sinha S, Rossi MP, Mattia D, Gogotsi Y, Bau HH (2007) Induction and measurement of minute flow rates through nanopipes. *Phys Fluids* 19(1):013603.
89. Rossi MP, et al. (2004) Environmental scanning electron microscopy study of water in carbon nanopipes. *Nano Lett* 4(5):989–993.
90. Glavatskiy KS, Bhatia SK (2016) Thermodynamic resistance to matter flow at the interface of a porous membrane. *Langmuir* 32(14):3400–3411.
91. Sisan TB, Lichter S (2011) The end of nanochannels. *Microfluid Nanofluidics* 11(6): 787–791.

Downloaded from https://www.pnas.org by 147.161.165.28 on March 4, 2025 from IP address 147.161.165.28.